NANO LETTERS

pubs.acs.org/NanoLett

Letter

Nonlocal Screening Dictates the Radiative Lifetimes of Excitations in Lead Halide Perovskites

Yoonjae Park, Amael Obliger, and David T. Limmer*

Cite This: *Nano Lett.* 2022, 22, 2398−2404

Read Online

ACCESS | Metrics & More | Article Recommendations | Supporting Information

ABSTRACT: We use path integral molecular dynamics simulations and theory to elucidate the interactions between charge carriers, as mediated by a lead halide perovskite lattice. We find that the charge−lattice coupling of $MAPbI_3$ results in a repulsive interaction between electrons and holes at intermediate distances. The effective interaction is understood using a Gaussian field theory, whereby the underlying soft, polar lattice contributes a nonlocal screening between quasiparticles. Path integral calculations of this nonlocal screening model are used to rationalize the small exciton binding energy and low radiative recombination rate observed experimentally and are compared to traditional Wannier−Mott and Fröhlich models, which fail to do so. These results clarify the origin of the high power conversion efficiencies in lead halide perovskites. Emergent repulsive electron−hole interactions provide a design principle for optimizing soft, polar semiconductors.

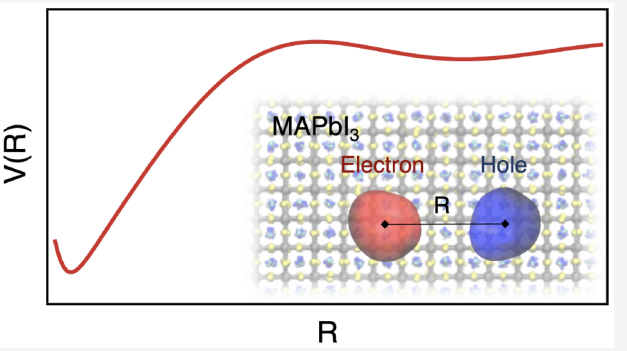

KEYWORDS: *Lead halide perovskite, excitons, charge carrier lifetime, path integral molecular dynamics, Gaussian field theory*

Lead halide perovskites are a class of materials that have unique photophysical properties resulting from their soft, polar lattices. They have vanishingly small exciton binding energies and despite modest mobilities, have large free carrier diffusion lengths resulting from exceptionally long carrier lifetimes.[1−3] These properties make lead halide perovskites ideal materials for photovoltaic devices.[4−6] Many of their optoelectronic properties have been thought to arise from electron−phonon coupling, as the largely ionic bonding of the lead halides admit strong Coulomb interactions between free charges and the lattice.[7] It has been conjectured that polaronic effects in particular[8−10] act to protect free charges from recombination and screen their interactions, reducing exciton binding energies.[9] However, the significant anharmonicity of the perovskite lattice has made uncovering the molecular origin of these properties difficult.[11−14]

Here, we apply path integral molecular dynamics[15,16] to study an atomistic model of quasiparticles embedded in a $MAPbI_3$ lattice, in order to understand how a fluctuating lattice affects its electronic properties. Much recent effort has gone into understanding the effects of the lattice on the excitonic properties of perovskites computationally[17−20] and analytically.[18,21] However, unlike traditional polar semiconductors where lattice fluctuations can be described by a harmonic approximation, the tilting and rocking motions of the inorganic octahedra[14] and nearly free motions of the A-site cations[12,13] render the lattice highly anharmonic. This complicates the simplification to traditional model Hamiltonians like the Fröhlich model or its generalizations.[20,22] Attempts to include lattice effects into *ab initio* based approaches have been developed, but these are difficult to extend to the time and length scales necessary to explain the nature of how photogenerated electrons and holes bind, dissociate, and recombine.[23] Using an explicit atomistic representation of the lattice surrounding the quasiparticles allows us to go beyond simplified models. Employing path integral calculations allows us to consider finite temperature effects directly on diffusive time and length scales. These simulations motivate a field theory to describe the effective electron−hole interactions that dictate the emergent optical properties of the perovskites. With these simulations and theory, we are able to elucidate the origin of low exciton binding energies and recombination rates as a consequence of a nonlocal screening from the lattice.

We consider a system of an electron−hole pair, interacting with a $MAPbI_3$ perovskite in its cubic phase employing a fully atomistic description of the lattice. The full system Hamiltonian, $\mathcal{H}$, consists of electronic, lattice, and interaction pieces, $\mathcal{H} = \mathcal{H}_{el} + \mathcal{H}_{l} + \mathcal{H}_{int}$. The highly dispersive bands of $MAPbI_3$ allow us to make an effective mass approximation, so that the electronic Hamiltonian is defined as

Received: January 10, 2022
Revised: February 25, 2022
Published: March 2, 2022

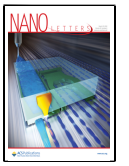

https://doi.org/10.1021/acs.nanolett.2c00077
Nano Lett. 2022, 22, 2398−2404

$$\mathcal{H}_{el} = \frac{\hat{\mathbf{p}}_e^{\,2}}{2m_e} + \frac{\hat{\mathbf{p}}_h^{\,2}}{2m_h} - \frac{e^2}{4\pi\epsilon_0\epsilon_\infty|\hat{\mathbf{r}}_e - \hat{\mathbf{r}}_h|} \quad (1)$$

where the subscripts e and h indicate electron and hole, $\hat{\mathbf{p}}$ and $\hat{\mathbf{r}}$ are the momentum and position operators, $m_e/m = m_h/m = 0.2$ are the band masses of the quasiparticles taken from recent GW calculations in units of the bare electron mass m,[24] ε_0 is the vacuum permittivity, and ϵ_∞ is the optical dielectric constant for charge e. For the lattice, we use an atomistic model developed by Mattoni et al. that has been demonstrated to reproduce the structural and dielectric properties of lead halide perovskites.[25,26] Its Hamiltonian is decomposable as

$$\mathcal{H}_l = \sum_{i=1}^{N} \frac{\hat{\mathbf{p}}_i^{\,2}}{2m_i} + U_l(\hat{\mathbf{r}}^N) \quad (2)$$

where $\hat{\mathbf{p}}_i$, $\hat{\mathbf{r}}_i$, and m_i are the momentum, position, and mass of ith atom, N is the total number of atoms in the lattice, and $U_l(\hat{\mathbf{r}}^N)$ is the pairwise interaction potential between atoms with configuration $\hat{\mathbf{r}}^N = \{\hat{\mathbf{r}}_1, \hat{\mathbf{r}}_2, ..., \hat{\mathbf{r}}_N\}$. The potential includes electrostatic and excluded volume interactions. The charge−lattice interaction term is given by $\mathcal{H}_{int} = U_{e,l}(\hat{\mathbf{r}}_e, \hat{\mathbf{r}}^N) + U_{h,l}(\hat{\mathbf{r}}_h, \hat{\mathbf{r}}^N)$ where $U_{e,l}$ and $U_{h,l}$ denote sums of pseudopotentials. Consistent with the largely ionic nature of $MAPbI_3$, we employ pseudopotentials of the form of short-ranged truncated Coulomb potentials, with a cutoff radii chosen as the ionic radii of each species.[27−29]

As the atoms are heavy and we are largely interested in room temperature behavior, we adopt a classical description of the $MAPbI_3$ lattice. We discuss below corrections to this classical approximation in the harmonic lattice limit. For the two light quasiparticles, however, we employ a path integral description to account for quantum mechanical effects important even at room temperature. Such a quasiparticle path integral approach has been employed previously to study lattice effects in the lead halides and trapping in other semiconductors.[30−33] The partition function, $\mathcal{Z}$, for the composite system can be written as

$$\mathcal{Z} = \int \mathcal{D}[\mathbf{r}_e, \mathbf{r}_h, \mathbf{r}^N] e^{-\mathcal{S}[\mathbf{r}_e, \mathbf{r}_h, \mathbf{r}^N]/\hbar} \quad (3)$$

with the action $\mathcal{S}[\mathbf{r}_e, \mathbf{r}_h, \mathbf{r}^N] = \mathcal{S}_{el} + \mathcal{S}_l + \mathcal{S}_{int}$. The corresponding imaginary time path action for the electronic part becomes

$$\mathcal{S}_{el} = \int_\tau \frac{m_e \dot{\mathbf{r}}_{e,\tau}^{\,2}}{2} + \frac{m_h \dot{\mathbf{r}}_{h,\tau}^{\,2}}{2} - \frac{e^2}{4\pi\epsilon_0\epsilon_\infty|\mathbf{r}_{e,\tau} - \mathbf{r}_{h,\tau}|} \quad (4)$$

where the imaginary time τ is defined over the interval 0 to $\beta\hbar$, $\beta^{-1} = k_B T$, T is temperature, k_B is Boltzmann's constant, and $\hbar$ is Planck's constant. The velocity and position of electron/hole are denoted $\dot{\mathbf{r}}_{e/h,\tau}$ and $\mathbf{r}_{e/h,\tau}$. Under the assumption of a classical lattice, the contributions to the path action from $MAPbI_3$ and its interaction with the quasiparticles become $\mathcal{S}_l = \beta\hbar\mathcal{H}_l$ and

$$\mathcal{S}_{int} = \int_\tau U_{e,l}(\mathbf{r}_{e,\tau}, \mathbf{r}^N) + U_{h,l}(\mathbf{r}_{h,\tau}, \mathbf{r}^N) \quad (5)$$

an integral over the pseudopotentials. When the path action is discretized into a finite number of imaginary time slices, the classical counterpart of each quantum particle becomes a ring polymer consisting of beads connected by harmonic springs.[34]

We perform molecular dynamics (MD) simulations of two ring polymers with 1000 beads representing the electron and hole and an $MAPbI_3$ lattice with 40 × 15 × 15 unit cells at 300 K. The large system size is necessary in order to ensure that self-interaction errors between the quasiparticles are minimized. This atomistic description allows us to capture all orders of interaction between the quasiparticles and the $MAPbI_3$ lattice, free of low temperature harmonic approximations. The simulation details including pseudopotentials and the force field of the lattice can be found in Supporting Information (SI section I).

To analyze the emergent exciton interaction resulting from the collective motions in $MAPbI_3$, we compute the free energy between electron and hole using Umbrella sampling with the Weighted Histogram Analysis Method.[35] We compute the reversible work to move two charge centers relative to each other

$$\beta F(R) = -\ln\langle\delta(R - |\mathbf{r}_e^c - \mathbf{r}_h^c|)\rangle \quad (6)$$

where R is the distance between the electron and hole centroid $\mathbf{r}_{e/h}^c$, $\delta(x)$ is Dirac's delta function, and $\langle ... \rangle$ represents an ensemble average. Simulation snapshots are shown in Figure 1a,b, where spatially delocalized charges extend with a radius of gyration between 1.5 and 3 nm. Figure 1c shows $F(R)$, which is nonmonotonic. The free energy exhibits a minima at $R = 0$ reflecting the binding of the electron−hole pair into an exciton, a plateau at large R, and a barrier at intermediate $R \approx 8$ nm. The binding energy is large due to the neglect of polarizability in this description of the lattice. Considering the bare

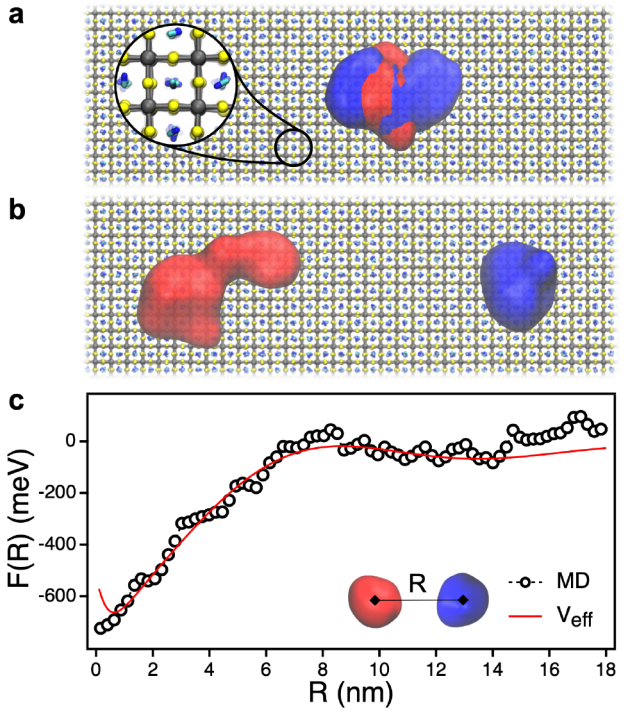

Figure 1. Quasiparticle path integral molecular dynamics simulations. Representative snapshots of the simulation of electron (red) and hole (blue) with the $MAPbI_3$ lattice where the electron and hole are (a) close to and (b) far from each other. Zoomed in structure in (a) represents the $MAPbI_3$ lattice where gray, yellow, and blue atoms represent Pb^{2+}, I^-, and MA^+, respectively. (c) Free energy between electron and hole as a function of the distance between quasiparticle centroids from molecular dynamics simulation (black circles) and an effective exciton interaction from eq 13 (red solid line) with parameters as $\varepsilon^* = 5$, $l_s = 2.47$ nm, and $l_c = 1.26$ nm.

https://doi.org/10.1021/acs.nanolett.2c00077
Nano Lett. 2022, 22, 2398−2404

Coulomb potential is a monotonic function, the repulsive interaction found in Figure 1c at intermediate electron−hole distances must arise from the lattice. An effective electron−hole repulsion has been speculated in lead halide perovskites previously[36−38] but had defied direct observation or theoretical validation.

In order to understand the emergent lattice effects on the electron−hole interaction and surprising intermediate repulsion, we assume that the fluctuations of the lattice are well described by a Gaussian field. Such Gaussian field theories underpin a number of standard effective interactions including dielectric continuum theory and the Casimir effect.[39−41] A Gaussian approximation in this context is analogous to the quasi-harmonic approach[42] where it is assumed that while the lattice is anharmonic, it responds linearly.[43,44] We consider approximating the lattice by an effective polar displacement field, $\mathbf{u}_{\mathbf{k},\tau}$, which is expected to be correlated with local bending and rocking motions of the octahedra.[45] Within the Gaussian field approximation, the path action for the lattice becomes

$$\mathcal{S}_{\mathrm{l}} \approx \frac{1}{2}\int_{\tau}\int_{\tau'}\int_{\mathbf{k}} \mathbf{u}_{\mathbf{k},\tau}\chi^{-1}_{\mathbf{k},\tau-\tau'}\mathbf{u}_{-\mathbf{k},\tau'} \tag{7}$$

where $\chi_{\mathbf{k},\tau-\tau'} = \langle \mathbf{u}_{\mathbf{k},\tau}\mathbf{u}_{-\mathbf{k},\tau'}\rangle$ is the susceptibility at wave vector $\mathbf{k}$ and imaginary time displacement $\tau - \tau'$. The susceptibility is determined by a phonon dispersion relationship only in the limit of zero temperature, and generally reflects the correlations within the effective polar displacement field.[46] Consistent with the Coulombic pseudopotentials used in the MD simulations, we take the coupling between the charges and the lattice to be linear

$$\mathcal{S}_{\mathrm{int}} \approx \int_{\tau}\int_{\mathbf{k}} \mathbf{u}_{\mathbf{k},\tau}\lambda\frac{\mathrm{e}^{\mathrm{i}\mathbf{k}\cdot\mathbf{r}_{\mathrm{e},\tau}} - \mathrm{e}^{\mathrm{i}\mathbf{k}\cdot\mathbf{r}_{\mathrm{h},\tau}}}{k} \tag{8}$$

and described by a Fröhlich-like interaction,[47] where λ is a Fröhlich coupling constant. The lattice variables can be integrated out, leaving a Gaussian approximation to the partition function, $\mathcal{Z}_{\mathrm{G}}$,

$$\begin{aligned}\mathcal{Z}_{\mathrm{G}} &= \int \mathcal{D}[\mathbf{r}_{\mathrm{e}}, \mathbf{r}_{\mathrm{h}}, \mathbf{u}_{\mathbf{k}}]\mathrm{e}^{-\mathcal{S}_{\mathrm{all}}[\mathbf{r}_{\mathrm{e}},\mathbf{r}_{\mathrm{h}},\mathbf{u}_{\mathbf{k}}]/\hbar} \\ &= \mathcal{Z}_{\mathrm{l}}\int \mathcal{D}[\mathbf{r}_{\mathrm{e}}, \mathbf{r}_{\mathrm{h}}]\mathrm{e}^{-\mathcal{S}_{\mathrm{el}}/\hbar}\mathrm{e}^{-\mathcal{S}_{\mathrm{eff}}[\mathbf{r}_{\mathrm{e}},\mathbf{r}_{\mathrm{h}}]/\hbar}\end{aligned} \tag{9}$$

where $\mathcal{Z}_{\mathrm{l}}$ is the partition function for a displacement field without couplings to the charges. This integration results in an effective path action of the form (see the SI for details)

$$\mathcal{S}_{\mathrm{eff}} = -\sum_{i,j}\int_{\tau}\int_{\tau'}\int_{\mathbf{k}}\Gamma_{ij}\chi_{\mathbf{k},\tau,\tau'}\frac{|\lambda|^2}{2k^2}\mathrm{e}^{\mathrm{i}\mathbf{k}\cdot|\mathbf{r}_{i,\tau}-\mathbf{r}_{j,\tau'}|} \tag{10}$$

where $i, j \in \{e, h\}$ and Γ_{ij} takes the value of $\Gamma_{ij} = 1$ if $i = j$ and $\Gamma_{ij} = -1$ if $i \neq j$.

The susceptibility $\chi_{\mathbf{k},\tau}$ is proportional to a dielectric function evaluated in the absence of the quasiparticles. Different functional forms of its imaginary time and wavevector dependence imply different ways in which the lattice can screen the quasiparticles. In the classical limit,[48] $\chi_{\mathbf{k},\tau} = \chi_{\mathbf{k}}\delta(\tau)$, eqs 4, 10, and 12, imply an effective interaction between the electron and hole,

$$\hat{V}_{\mathrm{eff}}(\mathbf{k}) = -\frac{1}{k^2}\left[\frac{e^2}{\epsilon_0\epsilon_\infty} - \chi_{\mathbf{k}}|\lambda|^2\right] \tag{11}$$

which is a sum of the bare interaction, here screened by $\epsilon_\infty = 4.5$,[49] and the contribution from the lattice proportional to $\chi_{\mathbf{k}}$. In the zero wavevector limit, this is a constant, and if taken as $\chi_{\mathbf{k}}|\lambda|^2 = e^2/\epsilon_0(1/\epsilon_\infty - 1/\epsilon_{\mathrm{r}})$, we recover the Wannier−Mott model of a exciton. With an effective dielectric constant $\epsilon_{\mathrm{r}} = 6.1$,[24] this local, *static* screening is manifestly insufficient to produce the repulsive interaction observed from the free energy calculations. Rather an explicit $\mathbf{k}$ dependence to $\chi_{\mathbf{k}}$ is required.

Using explicit MD simulations of the bulk classical $MAPbI_3$ lattice, we find $\chi_{\mathbf{k}}$ is well approximated by

$$\chi_{\mathbf{k}} \approx \frac{\chi_0}{1 - l_{\mathrm{s}}^2\mathbf{k}^2 + l_{\mathrm{s}}^2 l_{\mathrm{c}}^2\mathbf{k}^4} \tag{12}$$

characterized by three positive real parameters, χ_0, l_{s}, and l_{c}. This functional form includes a single resonant peak and is assumed isotropic on length scales greater than the lattice spacing. The resonant peak results from the negative second-order coefficient and manifests the double well potential of the optical mode.[18] Performing the inverse Fourier transform gives an effective potential

$$V_{\mathrm{eff}}(r) = -\frac{e^2}{4\pi\epsilon_0 r}\left[\frac{1}{\epsilon_\infty} + \frac{1}{\epsilon^*} + \frac{\gamma}{4\delta\epsilon^*}\mathrm{e}^{-r\delta}\sin[r\gamma - \theta]\right] \tag{13}$$

where r is the distance between two charges. Details of the derivation with analytic expressions for $1/\epsilon^*$, $\gamma^{-1} \approx \sqrt{2}\,l_{\mathrm{c}}$, $\delta^{-1} \approx 2l_{\mathrm{c}}/\sqrt{1 - l_{\mathrm{s}}/2l_{\mathrm{c}}}$, and $\theta = \arctan[2\delta/\gamma]$ are shown in the SI section II. This form is plotted in Figure 1c and provides an excellent fit at large r to the free energy from the MD simulation. We refer to this effective electron−hole interaction arising from spatially dependent screening from the $MAPbI_3$ lattice as *nonlocal* screening.[50] The theory clarifies that the nonmonotonic interaction potential results from deformations generated within the lattice due to the charges. At specific characteristic distances these deformations are sufficiently unfavorable that the electron and hole are effectively repelled from each other.

This effective interaction in eq 13 is distinct from what has been considered previously by Pollmann and Buttner,[51] and by Gerlach and Luczak[48] in which coupling to a single dispersionless optical phonon results in a excitonic polaron that screens the bare Coulomb potential. In their approximation, the polar displacement field is treated quantum mechanically by including a τ dependence of the susceptibility. In Pollmann and Buttner's work, this is taken as the bare susceptibility,

$$\chi_{\mathbf{k},\tau} = \frac{1}{2\omega}\mathrm{e}^{-\omega|\tau|} \tag{14}$$

where the phonon mode is characterized by a single longitudinal optical frequency ω. Plugging eq 14 into eq 10, we obtain the effective path action

$$\mathcal{S}_{\mathrm{eff}} = -\sum_{i,j}\Gamma_{ij}\frac{\alpha\omega^2\hbar^{3/2}}{\sqrt{8m_{ij}\omega}}\int_{\tau}\int_{\tau'}\frac{\mathrm{e}^{-\omega|\tau-\tau'|}}{|\mathbf{r}_{i,\tau} - \mathbf{r}_{j,\tau'}|} \tag{15}$$

where we have written $|\lambda|^2$ in the traditional Fröhlich form, introducing α as the dimensionless coupling constant. Pollmann and Buttner further approximate this *dynamic* screening approach in order to obtain a closed form effective potential. Their potential is an exponentially screened

https://doi.org/10.1021/acs.nanolett.2c00077
Nano Lett. 2022, 22, 2398−2404

Coulomb potential in the classical limit with a screening length given by the polaron radus.[51] While for certain parameters it is possible that the Pollmann−Buttner potential is repulsive,[36] employing known values for α = 1.72 and ω = 40 cm^{-1} for $MAPbI_3$,[49] the resultant effective potential is monotonic and inconsistent with our MD result. Analogous approaches including sums of two or three dispersionless phonons similarly fail to describe a repulsive interaction. Treating the susceptibility variationally, Gerlach and Luczak[48] provided a more flexible description of the lattice, but the lack of a wavevector dependence to χ still prohibits an intermediate length scale repulsion.

To investigate the implication of a nonlocal screening on the observable properties of $MAPbI_3$, we simulated an electron and hole pair using our quasiparticle path integral approach under (i) static, (ii) dynamic, and (iii) nonlocal screenings. In each case, we employed known experimental parameters for the dielectric constants, optical frequencies, and effective masses and thus expect our results to be quantitatively accurate. To our knowledge the **k**-dependent dielectric susceptibility has not been reported for $MAPbI_3$, so we parametrized the nonlocal screening interaction using our MD results. For each case, we extract the exciton binding energies and bimolecular recombination rates as both have been difficult to reconcile theoretically.[52]

The exciton binding energy, ΔE_B is definable within our path integral framework as

$$\Delta E_B = \lim_{T\to 0} \min_R \Delta F(R) \tag{16}$$

and to evaluate it we computed the free energy $\Delta F(R) = F(R) - F(\infty)$ at a variety of temperatures ranging from 100 to 400 K and extrapolate its value to 0 K (SI Figure S2). Representative free energies at T = 300 K are shown in Figure 2a. As anticipated from the theory, we find that both dynamic and nonlocal screening reduce the effective attraction between the electron and hole, but only the nonlocal screening results in a barrier to recombination.

The extrapolated binding energies are summarized in Table 1. Within the static screening approach, the exciton is hydrogenic, and the binding energy is given by $\Delta E_B^s = \mu e^4/2(4\pi\epsilon_0\epsilon_r)^2\hbar^2$ where μ is a reduced mass of the electron and hole. The large decrease in binding energy under dynamic screening reflects the polaronic effect. Since the experimentally derived value of α is relatively small,[49] we find the change to the binding energy is well approximated by first-order perturbation theory, yielding the known Fröhlich result, $\Delta E_B^d = \Delta E_B^s - 2\alpha\hbar\omega$.[53] This reduction in the binding energy is consistent with recent Bethe−Salpeter calculations with perturbative electron−phonon interactions,[23] but higher than experimental estimates.[54] The reduction in the binding energy from the nonlocal screening is 12 meV, which is close to a prediction assuming hydrogenic 1s orbits, 17 meV.

In the low temperature limit, the classical lattice approximation employed to construct the nonlocal screening model is no longer valid. In this limit, quantization of the phonons can lead to hybridization and polaron formation. To estimate the quantum mechanical effect of phonons in this model, we have adopted a hybrid approach where we have added a single optical phonon as done in the dynamical approximation, to the effective potential description deduced form the classical lattice simulations. The dynamical mode is treated analogously as eq 15, while the effective potential is

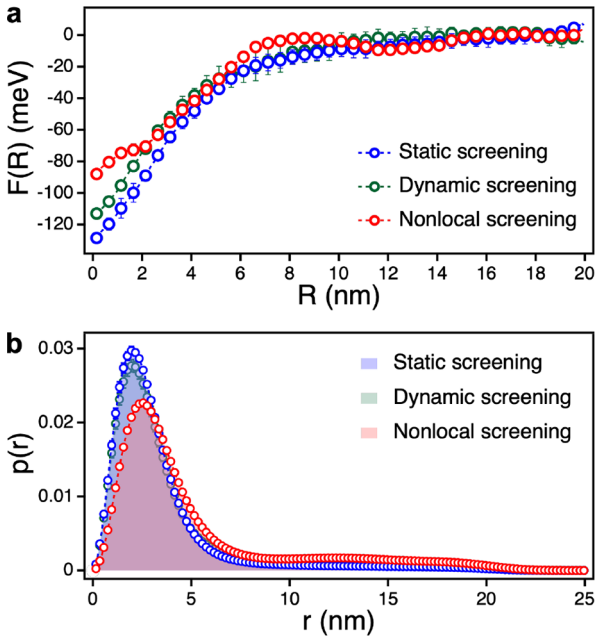

Figure 2. Implications of different screening models from explicit path integral simulations with electron and hole quasiparticles. (a) Free energy as a function of the distance between quasiparticle centroids at 300 K under static (blue), dynamic (green), and nonlocal (red) screening models. (b) Radial probability distribution for electron and hole, with the same color scheme as in (a).

Table 1. Exciton Binding Energy ΔE_B and Carrier Lifetime τ_r Estimated Using Different Screening Models

screenings	static	dynamic	nonlocal
ΔE_B (meV)	50.4	36.9	38.1
τ_r (ns)	13.5	35.5	78.1

assumed to be constant at low temperatures and reflective of dynamic disorder. Treating both of these effects yields a binding energy of 20.8 meV in very good agreement with experiment.[54,55]

The bimolecular recombination rate, k_r is defined as the rate of change of the concentration of free charges,

$$\frac{d\rho_e}{dt} = -k_r\rho_e\rho_h \tag{17}$$

through the reaction $e^- + h^+ \rightarrow \hbar\nu$, where $\rho_{e/h}$ is the concentration of free electrons/holes. At typical working excitation densities for $MAPbI_3$ based photovoltaics, radiative recombination is the limiting factor determining the charge carrier lifetime.[52] We can evaluate k_r using Fermi's golden rule for spontaneous emission, with an effective mass approximation.[56−59] Within our quasiparticle path integral framework, the rate is given by a constant times a ratio of path partition functions,[60]

$$k_r = \frac{e^2\sqrt{\epsilon_\infty}E_{gap}^{\ 2}}{2\pi\epsilon_0\hbar^2c^3\mu}\frac{\mathcal{Z}_c}{\mathcal{Z}} \tag{18}$$

where E_{gap} = 1.64 eV is the band gap energy for $MAPbI_3$ and c is the speed of light. The subscript c on $\mathcal{Z}_c$ stands for combined path integral in which the two separate imaginary time paths are placed together to form a single, radiating path

https://doi.org/10.1021/acs.nanolett.2c00077
Nano Lett. 2022, 22, 2398−2404

by linking same imaginary time slices. The ratio of path partition functions can be evaluated as

$$\frac{\mathcal{Z}_c}{\mathcal{Z}} = 4\pi \int \mathrm{d}R\ R^2 \langle e^{\Delta S/\hbar} \rangle_R e^{-\beta \Delta F(R)} \tag{19}$$

where we replace the ratio of partition functions by an exponential average at fixed R of the difference in path action $\Delta S = S - S_c$ (SI eq S13).

The change in action is a reporter on the overlap between the electron and hole wave functions. The electron and hole radial probability distribution is described in Figure 2b, illustrating that the nonlocal screening effect increases the average distance between electron and hole. This is distinct from the effect of the dynamic screening, which is consistent with the small value of α, leaves the electronic distribution largely unaltered from the simple Wannier, static screening model. The decrease in electron hole overlap results in a nearly order of magnitude decrease in k_r using the nonlocal screening theory relative to the static screening theory. For the nonlocal screening theory, we find $k_r = 1.3 \times 10^{-10}$ cm^3/s, in excellent agreement with photoluminescence lifetime measurements.[52]

Assuming the only loss mechanism is due to bimolecular recombination, the lifetime of an electron hole pair is computable from $\tau_r = 1/k_r\rho_e$. Summarized in Table 1 for $\rho_e = 10^{17}$/cm^3 are lifetime estimates using the different screening models. Both standard polaronic effects incorporated into the dynamic screening model as well as the nonlocal screening model increase the lifetimes of free charge carriers; however, the contribution of a nonlocal screening obtained from the $MAPbI_3$ lattice is much more significant. The details on the bimolecular recombination rate calculations are in the SI section III.

By comparing these different simplified models that account for charge−lattice interactions, we find that the ability of the $MAPbI_3$ lattice to nonlocally screen quasiparticles is sufficient to explain the particularly low exciton binding energy and recombination rate. Only this screening kernel in our unified Gaussian field theory formalism can suppress the electron−hole overlap enough to explain the anomalously long free carrier lifetime with weak lattice coupling strength. The particular nonlocal screening adopted here was deduced directly from explicit atomistic molecular dynamics simulations using a quasiparticle path integral framework. This framework is uniquely able to study the thermodynamics of this quasiparticle−lattice system at finite temperature.

The adoption of a spatially dependent screening is consistent with a growing literature pointing to the importance of dynamic disorder in lead halide perovskites.[61−63] As it is the wave-vector-dependent dielectric susceptibility of the bulk ground state lattice that enters into the theory presented above, experimental measurements of such properties could afford a means of assessing potential materials with similarly long radiative lifetimes. Further, the barrier to bringing electrons and holes together we have discovered here undoubtedly has implications apart from offering an explanation of the particular high power conversion efficiencies of $MAPbI_3$. For example, this repulsion may help explain observations of antibinding of biexcitons.[37,38] The identification of a repulsive electron−hole interaction generated from the soft, polar modes of the perovskite lattice offers a key new design principle for photovoltaic materials. Searching for other systems that admit this type of interaction represents a promising new direction for materials discovery.

■ ASSOCIATED CONTENT

Supporting Information

The Supporting Information is available free of charge at https://pubs.acs.org/doi/10.1021/acs.nanolett.2c00077.

Details of simulations, derivation of effective electron−hole interaction, and the bimolecular recombination rate with path integral framework, tables of potential parameters, figures of susceptibility plots, ΔF vs temperature, ratio of partition functions vs number of beads, and schematic illustration of action paths (PDF)

■ AUTHOR INFORMATION

Corresponding Author

David T. Limmer − *Department of Chemistry, University of California, Berkeley, California 94720, United States; Materials Science Division, Lawrence Berkeley National Laboratory, Berkeley, California 94720, United States; Chemical Science Division, Lawrence Berkeley National Laboratory, Berkeley, California 94720, United States; Kavli Energy NanoScience Institute, Berkeley, California 94720, United States;* orcid.org/0000-0002-2766-0688; Email: dlimmer@berkeley.edu

Authors

Yoonjae Park − *Department of Chemistry, University of California, Berkeley, California 94720, United States*

Amael Obliger − *Department of Chemistry, University of California, Berkeley, California 94720, United States;* Present Address: ISM, Université Bordeaux, CNRS, Talence, France

Complete contact information is available at: https://pubs.acs.org/10.1021/acs.nanolett.2c00077

Notes

The authors declare no competing financial interest.

■ ACKNOWLEDGMENTS

This work was supported by the U.S. Department of Energy, Office of Science, Office of Basic Energy Sciences, Materials Sciences and Engineering Division under Contract No. DE-AC02-05-CH11231 within the Physical Chemistry of Inorganic Nanostructures Program (No. KC3103). This research used resources of the National Energy Research Scientific Computing Center (NERSC), a U.S. Department of Energy Office of Science User Facility. Y.P. also acknowledges Kwanjeong Educational Foundation. D.T.L. acknowledges the Alfred P. Sloan Foundation.

■ REFERENCES

(1) de Quilettes, D. W.; Vorpahl, S. M.; Stranks, S. D.; Nagaoka, H.; Eperon, G. E.; Ziffer, M. E.; Snaith, H. J.; Ginger, D. S. Impact of microstructure on local carrier lifetime in perovskite solar cells. *Science* **2015**, *348*, 683−686.

(2) Wehrenfennig, Christian; Eperon, Giles E.; Johnston, Michael B.; Snaith, Henry J.; Herz, Laura M. High Charge Carrier Mobilities and Lifetimes in Organolead Trihalide Perovskites. *Adv. Mater.* **2014**, *26*, 1584−1589.

(3) Stranks, Samuel D; Eperon, Giles E; Grancini, Giulia; Menelaou, Christopher; Alcocer, Marcelo JP; Leijtens, Tomas; Herz, Laura M; Petrozza, Annamaria; Snaith, Henry J Electron-hole diffusion lengths exceeding 1 micrometer in an organometal trihalide perovskite absorber. *Science* **2013**, *342*, 341−344.

(4) Xing, Guichuan; Mathews, Nripan; Lim, Swee Sien; Yantara, Natalia; Liu, Xinfeng; Sabba, Dharani; Grätzel, Michael; Mhaisalkar, Subodh; Sum, Tze Chien Low-temperature solution-processed wavelength-tunable perovskites for lasing. *Nat. Mater.* **2014**, *13*, 476−480.
(5) Sutton, Rebecca J.; Eperon, Giles E.; Miranda, Laura; Parrott, Elizabeth S.; Kamino, Brett A.; Patel, Jay B.; Hörantner, Maximilian T.; Johnston, Michael B.; Haghighirad, Amir Abbas; Moore, David T.; Snaith, Henry J. Bandgap-Tunable Cesium Lead Halide Perovskites with High Thermal Stability for Efficient Solar Cells. *Adv. Energy Mater.* **2016**, *6*, 1502458.
(6) Lee, Michael M; Teuscher, Joël; Miyasaka, Tsutomu; Murakami, Takurou N; Snaith, Henry J Efficient hybrid solar cells based on meso-superstructured organometal halide perovskites. *Science* **2012**, *338*, 643−647.
(7) Wang, He; Valkunas, Leonas; Cao, Thu; Whittaker-Brooks, Luisa; Fleming, Graham R Coulomb Screening and Coherent Phonon in Methylammonium Lead Iodide Perovskites. *J. Phys. Chem. Lett.* **2016**, *7*, 3284−3289.
(8) Zhu, X.-Y.; Podzorov, V. Charge Carriers in Hybrid Organic−Inorganic Lead Halide Perovskites Might Be Protected as Large Polarons. *J. Phys. Chem. Lett.* **2015**, *6*, 4758−4761.
(9) Chen, Y.; Yi, H. T.; Wu, X.; Haroldson, R.; Gartstein, Y. N.; Rodionov, Y. I.; Tikhonov, K. S.; Zakhidov, A.; Zhu, X. Y.; Podzorov, V. Extended carrier lifetimes and diffusion in hybrid perovskites revealed by Hall effect and photoconductivity measurements. *Nat. Commun.* **2016**, *7*, 12253.
(10) Cannelli, Oliviero; Nicola Colonna; Puppin, Michele; Rossi, Thomas C; Kinschel, Dominik; Leroy, Ludmila M D; Löffler, Janina; Budarz, James M.; March, Anne Marie; Doumy, Gilles; Al Haddad, Andre; Tu, Ming-Feng; Kumagai, Yoshiaki; Walko, Donald; Grigory Smolentsev; Krieg, Franziska; Boehme, Simon C; Kovalenko, Maksym V.; Chergui, Majed; Mancini, Giulia F Quantifying Photoinduced Polaronic Distortions in Inorganic Lead Halide Perovskite Nanocrystals. *J. Am. Chem. Soc.* **2021**, *143*, 9048−9059.
(11) Katan, Claudine; Mohite, Aditya D.; Even, Jacky. Entropy in halide perovskites. *Nat. Mater.* **2018**, *17*, 377.
(12) Motta, Carlo; El-Mellouhi, Fedwa; Kais, Sabre; Tabet, Nouar; Alharbi, Fahhad; Sanvito, Stefano Revealing the role of organic cations in hybrid halide perovskite CH3NH3PbI3. *Nat. Commun.* **2015**, *6*, 7026.
(13) Brivio, Federico; Frost, Jarvist M.; Skelton, Jonathan M.; Jackson, Adam J.; Weber, Oliver J.; Weller, Mark T.; Goñi, Alejandro R.; Aurélien, M.; Leguy, A.; Barnes, Piers R. F.; Walsh, Aron Lattice dynamics and vibrational spectra of the orthorhombic, tetragonal, and cubic phases of methylammonium lead iodide. *Phys. Rev. B* **2015**, *92*, 144308.
(14) Yang, Ruo Xi; Jonathan M Skelton, E Lora da Silva; Frost, Jarvist M; Walsh, Aron Spontaneous Octahedral Tilting in the Cubic Inorganic Cesium Halide Perovskites CsSnX 3 and CsPbX 3 (X = F, Cl, Br, I). *J. Phys. Chem. Lett.* **2017**, *8*, 4720−4726.
(15) Chandler, David; Wolynes, Peter G Exploiting the isomorphism between quantum theory and classical statistical mechanics of polyatomic fluids. *J. Chem. Phys.* **1981**, *74*, 4078−4095.
(16) Ceperley, David M Path integrals in the theory of condensed helium. *Rev. Mod. Phys.* **1995**, *67*, 279.
(17) Cho, Yeongsu; Berkelbach, Timothy C Optical Properties of Layered Hybrid Organic−Inorganic Halide Perovskites: A Tight-Binding GW-BSE Study. *J. Phys. Chem. Lett.* **2019**, *10*, 6189−6196.
(18) Schlipf, Martin; Poncé, Samuel; Giustino, Feliciano Carrier Lifetimes and Polaronic Mass Enhancement in the Hybrid Halide Perovskite CH3NH3PbI3 from Multiphonon Fröhlich Coupling. *Phys. Rev. Lett.* **2018**, *121*, 086402.
(19) Zheng, F.; Wang, L.-w. Large polaron formation and its effect on electron transport in hybrid perovskites. *Energy Environ. Sci.* **2019**, *12*, 1219−1230.
(20) Mayers, Matthew Z; Tan, Liang Z.; Egger, David A; Rappe, Andrew M; Reichman, David R How lattice and charge fluctuations control carrier dynamics in halide perovskites. *Nano Lett.* **2018**, *18*, 8041−8046.
(21) Menéndez-Proupin, E.; Beltrán Ríos, Carlos L.; Wahnón, P. Nonhydrogenic exciton spectrum in perovskite CH3NH3PbI3. *Physica status solidi (RRL) - Rapid Research Letters* **2015**, *9*, 559−563.
(22) Egger, David A; Bera, Achintya; Cahen, David; Hodes, Gary; Kirchartz, Thomas; Kronik, Leeor; Lovrincic, Robert; Rappe, Andrew M; Reichman, David R; Yaffe, Omer What remains unexplained about the properties of halide perovskites? *Adv. Mater.* **2018**, *30*, 1800691.
(23) Filip, Marina R.; Haber, Jonah B.; Neaton, Jeffrey B. Phonon Screening of Excitons in Semiconductors: Halide Perovskites and Beyond. *Phys. Rev. Lett.* **2021**, *127*, 067401.
(24) Cho, Yeongsu; Berkelbach, Timothy C Optical properties of layered hybrid organic−inorganic halide perovskites: A tight-binding gw-bse study. *J. Phys. Chem. Lett.* **2019**, *10*, 6189−6196.
(25) Mattoni, Alessandro; Filippetti, Alessio; Caddeo, Claudia Modeling hybrid perovskites by molecular dynamics. *J. Phys.: Condens. Matter* **2017**, *29*, 043001.
(26) Mattoni, A.; Caddeo, C. Dielectric function of hybrid perovskites at finite temperature investigated by classical molecular dynamics. *J. Chem. Phys.* **2020**, *152*, 104705.
(27) Parrinello, Michele; Rahman, Aneesur Study of an f center in molten kcl. *J. Chem. Phys.* **1984**, *80*, 860−867.
(28) Schnitker, Jürgen; Rossky, Peter J. An electron−water pseudopotential for condensed phase simulation. *J. Chem. Phys.* **1987**, *86*, 3462−3470.
(29) Kuharski, Robert A; Bader, Joel S.; Chandler, David; Sprik, Michiel; Klein, Michael L; Impey, Roger W Molecular model for aqueous ferrous−ferric electron transfer. *J. Chem. Phys.* **1988**, *89*, 3248−3257.
(30) Bischak, Connor G; Hetherington, Craig L; Wu, Hao; Aloni, Shaul; Frank Ogletree, D.; Limmer, David T; S Ginsberg, Naomi Origin of reversible photoinduced phase separation in hybrid perovskites. *Nano Lett.* **2017**, *17*, 1028−1033.
(31) Bischak, Connor G; Wong, Andrew B; Lin, Elbert; Limmer, David T; Yang, Peidong; S Ginsberg, Naomi Tunable polaron distortions control the extent of halide demixing in lead halide perovskites. *J. Phys. Chem. Lett.* **2018**, *9*, 3998−4005.
(32) Limmer, D. T.; Ginsberg, N. S. Photoinduced phase separation in the lead halides is a polaronic effect. *J. Chem. Phys.* **2020**, *152*, 230901.
(33) Remsing, Richard C; Bates, Jefferson E Effective mass path integral simulations of quasiparticles in condensed phases. *J. Chem. Phys.* **2020**, *153*, 121104.
(34) Habershon, S.; Manolopoulos, D. E.; Markland, T. E.; Miller, T. F. Ring-polymer molecular dynamics: Quantum effects in chemical dynamics from classical trajectories in an extended phase space. *Annu. Rev. Phys. Chem.* **2013**, *64*, 387−413.
(35) Kumar, S.; Rosenberg, J. M.; Bouzida, D.; Swendsen, R. H.; Kollman, P. A. THE weighted histogram analysis method for free-energy calculations on biomolecules. I. The method. *J. Comput. Chem.* **1992**, *13*, 1011.
(36) Emin, David Barrier to recombination of oppositely charged large polarons. *J. Appl. Phys.* **2018**, *123*, 055105.
(37) Lubin, G.; Yaniv, G.; Kazes, M.; Ulku, A. C.; Antolovic, I. M.; Burri, S.; Bruschini, C.; Charbon, E.; Yallapragada, V. J.; Oron, D. Resolving the controversy in biexciton binding energy of cesium lead halide perovskite nanocrystals through heralded single-particle spectroscopy. *ACS Nano* **2021**, *15*, 19581.
(38) Dana, Jayanta; Binyamin, Tal; Etgar, Lioz; Ruhman, Sanford Unusually strong biexciton repulsion detected in quantum confined cspbbr3 nanocrystals with two and three pulse femtosecond spectroscopy. *ACS Nano* **2021**, *15*, 9039.
(39) Song, Xueyu; Chandler, David; Marcus, R. A. Gaussian field model of dielectric solvation dynamics. *J. Phys. Chem.* **1996**, *100*, 11954−11959.
(40) Cox, Stephen J; Mandadapu, Kranthi K; Geissler, Phillip L Quadrupole-mediated dielectric response and the charge-asymmetric solvation of ions in water. *J. Chem. Phys.* **2021**, *154*, 244502.

https://doi.org/10.1021/acs.nanolett.2c00077
Nano Lett. 2022, 22, 2398−2404

(41) Li, Hao; Kardar, Mehran Fluctuation-induced forces between rough surfaces. *Phys. Rev. Lett.* **1991**, *67*, 3275.
(42) Brooks, Bernard R.; Janežič, Dušanka; Karplus, Martin Harmonic analysis of large systems. I. Methodology. *J. Comput. Chem.* **1995**, *16*, 1522−1542.
(43) Chandler, David Gaussian field model of fluids with an application to polymeric fluids. *Phys. Rev. E* **1993**, *48*, 2898.
(44) Reichman, David R; Voth, Gregory A Self-consistent harmonic theory of solvation in glassy systems: Classical solvation. *J. Chem. Phys.* **2000**, *112*, 3267−3279.
(45) Ferreira, A. C.; Paofai, Serge; Antoine, Létoublon; Ollivier, Jacques; Raymond, Stéphane; Bernard, Hehlen; Benoit, Rufflé; Cordier, Stéphane; Katan, Claudine; Even, Jacky; et al. Direct evidence of weakly dispersed and strongly anharmonic optical phonons in hybrid perovskites. *Commun. Phys.* **2020**, *3*, 48.
(46) Shih, Petra; Berkelbach, Timothy C. Anharmonic lattice dynamics from vibrational dynamical mean-field theory. *arXiv:2109.00028 [cond-mat.mtrl-sci]* **2021** (accessed Feb 1, 2022).
(47) Mozafari, Elham. *Theoretical Description of the Electron-Lattice Interaction in Molecular and Magnetic Crystals*; Linköping LiU-Tryck: Linköping, Sweden, 2016.
(48) Gerlach, B.; Luczak, F. Ground-state energy of an exciton-(LO) phonon system in two and three dimensions: General outline and three-dimensional case. *Phys. Rev. B* **1996**, *54*, 12841−12851.
(49) Sendner, Michael; Nayak, Pabitra K.; Egger, David A.; Beck, Sebastian; Müller, Christian; Epding, Bernd; Kowalsky, Wolfgang; Kronik, Leeor; Snaith, Henry J. Annemarie Pucci, and Robert Lovrinčić, "Optical phonons in methylammonium lead halide perovskites and implications for charge transport. *Materials Horizons* **2016**, *3*, 613−620.
(50) Kornyshev, A. A. Nonlocal screening of ions in a structurized polar liquid—new aspects of solvent description in electrolyte theory. *Electrochim. Acta* **1981**, *26*, 1−20.
(51) Pollmann, J.; Büttner, H. Effective hamiltonians and bindings energies of wannier excitons in polar semiconductors. *Phys. Rev. B* **1977**, *16*, 4480.
(52) Herz, Laura M Charge-carrier dynamics in organic-inorganic metal halide perovskites. *Annu. Rev. Phys. Chem.* **2016**, *67*, 65−89.
(53) Devreese, J. T. Fröhlich polarons. lecture course including detailed theoretical derivations. *arXiv:1012.4576 [cond-mat.other]* **2015** (accessed Feb 1, 2022).
(54) Galkowski, Krzysztof; Mitioglu, Anatolie; Miyata, Atsuhiko; Plochocka, Paulina; Oliver, Portugall; Eperon, Giles E; Wang, Jacob Tse-Wei; Stergiopoulos, Thomas; Stranks, Samuel D; Snaith, Henry J; et al. Determination of the exciton binding energy and effective masses for methylammonium and formamidinium lead tri-halide perovskite semiconductors. *Energy Environ. Sci.* **2016**, *9*, 962−970.
(55) D'Innocenzo, Valerio; Grancini, Giulia; Marcelo, J.; Alcocer, P.; Srimath Kandada, Ajay Ram; Stranks, Samuel D.; Lee, Michael M.; Lanzani, Guglielmo; Snaith, Henry J.; Petrozza, Annamaria Excitons versus free charges in organo-lead tri-halide perovskites. *Nat. Commun.* **2014**, *5*, 3586.
(56) Peter, Y. *Fundamentals of Semiconductor: Physics and Materials properties*; Springer: New York, 2010.
(57) Hamaguchi, Chihiro. *Basic Semiconductor Physics*; Springer: New York, 2009.
(58) Sahin, Mehmet; Koç, Fatih A model for the recombination and radiative lifetime of trions and biexcitons in spherically shaped semiconductor nanocrystals. *Appl. Phys. Lett.* **2013**, *102*, 183103.
(59) Fonoberov, Vladimir A.; Balandin, Alexander A. Excitonic properties of strained wurtzite and zinc-blende GaN/AlxGa1xN quantum dots. *J. Appl. Phys.* **2003**, *94*, 7178−7186.
(60) Wimmer, Michael.; Nair, S. V.; Shumway, J. Biexciton recombination rates in self-assembled quantum dots. *Phys. Rev. B* **2006**, *73*, 165305.
(61) Leguy, Aurélien; Goñi, Alejandro R; Frost, Jarvist M; Skelton, Jonathan; Brivio, Federico; Rodríguez-Martínez, Xabier; Weber, Oliver J; Pallipurath, Anuradha; Alonso, M Isabel; Campoy-Quiles, Mariano; et al. Dynamic disorder, phonon lifetimes, and the assignment of modes to the vibrational spectra of methylammonium lead halide perovskites. *Phys. Chem. Chem. Phys.* **2016**, *18*, 27051−27066.
(62) Schilcher, Maximilian J; Robinson, Paul J; Abramovitch, David J; Tan, Liang Z; Rappe, Andrew M; Reichman, David R; Egger, David A The significance of polarons and dynamic disorder in halide perovskites. *ACS Energy Letters* **2021**, *6*, 2162−2173.
(63) Quan, Li Na.; Park, Yoonjae.; Guo, Peijun.; Gao, Mengyu.; Jin, Jianbo.; Huang, Jianmei.; Copper, Jason K.; Adam, Schwartzberg.; Schaller, Richard.; Limmer, David T. Vibrational relaxation dynamics in layered perovskite quantum wells. *Proc. Natl. Acad. Sci. U. S. A.* **2021**, *118*, e2104425118.

https://doi.org/10.1021/acs.nanolett.2c00077
Nano Lett. 2022, 22, 2398−2404